1 **Surface formation, preservation, and history of low-porosity crusts at the**
2 **WAIS Divide site, West Antarctica.**

3 John M. Fegyveresi[1,2], Richard B. Alley[2], Atsuhiro Muto[3], Anaïs J. Orsi[4],
4 Matthew K. Spencer[5]
5
6 [1]Terrestrial and Cryospheric Sciences Branch, U.S. Cold Regions Research and
7 Engineering Laboratory (CRREL), Hanover, NH, 03755, USA.
8
9 [2]Dept. of Geosciences, and Earth and Environmental Systems Institute, Pennsylvania
10 State University, University Park, PA, 16802, USA.
11
12 [3]Dept. of Earth and Environmental Science, College of Science and Technology, Temple
13 University, Philadelphia, PA, 19122, USA.
14
15 [4]Laboratoire des Sciences du Climat et de l'Environnement, LSCE/IPSL, CEA-CNRS-
16 UVSQ, Université Paris-Saclay, F-91191, Gif-sur-Yvette, France.
17
18 [5]School of Physical Sciences, Lake Superior State University, Sault Sainte Marie, MI,
19 49783, USA.
20
21
22 *Correspondence to:*
23 J. M. Fegyveresi (fegy.john@gmail.com; john.m.fegyveresi@usace.army.mil)

24 **Key Words:**

25 • Antarctic snow surface, ice cores, field observations, snow-surface crusts, bubble-
26 free layers, vapor transport, firn properties, snow physics.

32                                    **Abstract**

33              Observations at the WAIS Divide site show that near-surface snow is strongly altered by

34       weather-related processes such as strong winds and temperature fluctuations, producing features

35       that are recognizable in the deep ice core. Prominent "glazed" surface crusts develop frequently at

36       the site during summer seasons. Surface, snow pit, and ice core observations made in this study

37       during summer field seasons from 2008-09 to 2012-13, supplemented by Automated Weather

38       Station (AWS) data with short and longwave radiation sensors, revealed that such crusts formed

39       during relatively low-wind, low-humidity, clear-sky periods with intense daytime sunshine. After

40       formation, such glazed surfaces typically developed cracks in a polygonal pattern likely from

41       thermal contraction at night. Cracking was commonest when several clear days occurred in

42       succession, and was generally followed by surface hoar growth; vapor escaping through the

43       cracks during sunny days may have contributed to the high humidity that favored nighttime

44       formation of surface hoar. Temperature and radiation observations show that daytime solar

45       heating often warmed the near-surface snow above the air temperature, contributing to upward

46       mass transfer, favoring crust formation from below, and then surface hoar formation. A simple

47       surface energy calculation supports this observation. Subsequent examination of the WDC06A

48       deep ice core revealed that crusts are preserved through the bubbly ice, and some occur in snow

49       accumulated during winters, although not as commonly as in summertime deposits. Although no

50       one has been on site to observe crust formation during winter, it may be favored by greater

51       wintertime wind-packing from stronger peak winds, high temperatures and steep temperature

52       gradients from rapid midwinter warmings reaching as high as -15°C, and perhaps longer intervals

53       of surface stability. Time-variations in crust occurrence in the core may provide paleoclimatic

54       information, although additional studies are required. Discontinuity and cracking of crusts likely

55       explain why crusts do not produce significant anomalies in other paleoclimatic records.

## 1: Introduction

Visual and thin-section examination of the WAIS Divide deep ice core from West Antarctica revealed an annual signal linked to bubble and grain characteristics [Fitzpatrick et al., 2014], but also numerous crusts. These crusts are bubble-free or nearly so, typically 1 mm or less and one grain in thickness, and are readily identified visually in bubbly ice (Fig. 1). Their presence in greater abundance than seen in most cores [e.g., Alley, 1988] motivated studies to understand their formation, possible influence on other paleoclimatic data, and potential for recording paleoclimatic conditions themselves.

Work by Orsi et al. [2015] and Mitchell et al. [2015] showed that no significant artifacts are introduced to paleoclimatic records by the WAIS Divide crusts. Here, we report additional studies showing that summertime crusts form under specific conditions linked to persistent high-pressure systems, so the time-series of crusts likely contains paleoclimatic information; however, many additional issues must be addressed before useful climate histories could be constructed confidently.

Bubble-free layers much thicker than the bubble-free crusts discussed here are sometimes observed in ice cores from warm sites, and provide evidence of refrozen meltwater [e.g., Das and Alley, 2005]. These are of interest as paleoclimatic records but have the potential to anomalously distort records of trapped gases or other components of ice cores. Refrozen meltwater can be identified by an excess of trapped heavy noble gases, so Orsi et al. [2015] analyzed WAIS Divide samples containing bubble-free crusts, finding that not enough meltwater was involved to significantly perturb records of other trace gases. Additionally, crusts might greatly modify gas trapping in the firn, but measured nitrogen-isotopic ratios at WAIS Divide show that gravitational fractionation occurs down to the normal trapping depth where normal amounts of air are trapped,

79    demonstrating that the crusts are not both impermeable and laterally extensive at shallow depth

80    [Mitchell et al., 2015; Battle et al., 2011].

81        Here, we report coordinated observations of crust formation over five summers (2008-09

82    to 2012-13) at the WAIS Divide site, involving daily observations of surface evolution, shallow

83    snow-pit studies with a 2-m pit at least once per year, insolation measurements, and near-surface

84    temperature profiling, supplemented with data from an on-site automated weather station (AWS).

85    We find that crusts form most commonly in the summer (45% greater occurrence), but do also

86    form in winter. In summer, crust formation primarily results from the effects of strong diurnal

87    temperature cycling under clear-sky, low-wind, relatively warm conditions. Wintertime

88    observations are not available, but the physical understanding gained from our summertime data

89    suggests hypotheses for formation. Time-trends in the occurrence of summertime crusts in the

90    core may reveal changes in the frequency of the persistent high-pressure conditions that generate

91    crusts, although additional work will be required to quantify this.

92    **2: Methods**

93        The main methods used are described here. Additional details are provided in Fegyveresi

94    [2015]. The surface was observed continually by one of us (JF) during the five field seasons

95    extending from 2008-09 to 2012-13 (Table 1). During each austral summer, a back-lit snow pit

96    was also prepared and studied (five total pits). All pits were sited within 1 km radius of the

97    primary ice-core drilling facility, but avoided regions disturbed by camp operations or the "drift

98    tail" of enhanced accumulation downwind of the camp. Following prior practice [e.g., Benson,

99    1962; Koerner, 1971; Alley, 1988], each sampling site involved excavating a pair of ~2 m cubic

100   pits separated by a wall ~0.5 m thick, with one pit left open to supply back-light, and the other a

101   roofed observation pit. Features such as crusts and hoar layers were easily identifiable from the

102    observation pit on the back-lit wall (Fig. 2). Pit walls were observed, mapped, sampled, and

103    photographed (tripod-mounted > ¼ s exposures). Each pit was oriented so the prevailing wind

104    direction, approximately north-south, ran from right-to-left along the back-lit wall.

105         An automatic weather station (AWS) on site at WAIS Divide (named Kominko-Slade in

106    the University of Wisconsin AWS system; Lazzara et al. [2012]), collected data on temperature,

107    air pressure, wind, and humidity starting in the 2009-10 season (all dates and times are GMT).

108    Beginning in 2011-12, upward-facing and downward-facing shortwave Li-Cor LI200

109    pyranometers were added initially 1 m above the surface to measure incoming and outgoing

110    shortwave radiation (0.4-1.1 μm spectral response). Both sensors were newly calibrated and

111    mounted in a cosine-corrected head (for solar angles up to 80°), with typical operational errors in

112    daylight of ±3% (max ±5%). A Kipp-Zonen CNR2 net radiometer with upward- and downward-

113    facing pyranometers and pyrgeometers was added on an AWS mounting arm during the 2012-13

114    season, in order to measure both net short and longwave radiation. This instrumentation replaced

115    the previous Li-Cor instrumentation. The pyranometers operated with a spectral response of 0.3 –

116    2.8 μm, operational errors of ±3.5 %, and sensitivity of 15.21 μV $W^{-1}$ $m^{-2}$, while the pyrgeometers

117    operated with a spectral response of 4.5–45 μm, operational errors of ±5.6 %, and a sensitivity of

118    12.52 μV $W^{-1}$ $m^{-2}$ respectively; typical impedances were ~7 ohms. All AWS relative humidity

119    values reported here are expressed in terms of saturation vapor pressure over ice and corrected for

120    low-temperature offsets (see Anderson, 1994).

121         Also during the 2012-13 season, we calibrated and installed five PRD (platinum

122    resistance detector) strings in the upper 5 m of snow in a 2 km survey line extending

123    approximately upwind (grid-west, true-north) starting ~50 meters from the on-site AWS. The

124    strings were designed by one of us (AM) following the procedures in Muto et al. [2011]. Each

125    sensor string was 5 m long and consisted of 16 individual PRDs (HEL-700 series; ±0.03°C

126    accuracy, ±0.18°C total combined error, including data-logger error) with denser sampling in the

127    shallower snow to capture the greater variability there (see also Supplemental Table S2). Sensor

128    calibration took place over a 60-minute period using a constantly-stirred ice-bath method, and

129    then the newly calibrated sensors were deployed incrementally over a 10-day period starting Dec.

130    15th. Deployment boreholes were drilled using a 4 cm diameter hand-auger, and then back-filled

131    once strings were installed. Campbell logging equipment (CR1000 data logger and AM/16/32

132    Multiplexer) and 12V sealed lead-acid batteries were housed in a foam-insulated wooden box

133    beside each borehole and just below the surface. The first string was placed 50 m from the AWS,

134    and the other strings were placed upwind of it by 10, 100, 1000, and 2000 m (Supplemental Table

135    S3). Measurements were taken every minute over the survey interval. Each 12V battery was

136    swapped out weekly with newly charged replacements to ensure that the sensor strings were

137    continually recording. During each site visit, we took photographs, and noted local

138    meteorological and surface conditions. Each sensor string took approximately 24 hours to

139    equilibrate with the surrounding snow following installation due to the backfilling of the open

140    boreholes with surface snow.

141        We studied crusts in the ice core as well as in the near-surface. As described in

142    Fitzpatrick et al. [2014], the entire deep core and various associated shallower cores were

143    inspected visually during core processing lines at the US National Ice Core Laboratory, primarily

144    by one of us (MS), but with some intercomparisons from other observers. The core was observed

145    on a light table in a darkened booth, and key features were noted on meter-length log books. The

146    crusts were easily visible as thin, glassy, bubble-free or nearly bubble-free layers (e.g. Fig. 1).

147        Annual cycles are visible in the bubbly part of the core, arising from the tendency for

148    near-surface processes to generate coarse-grained, low-density layers including depth hoar in

149    summer [Fitzpatrick et al., 2014; Fegyveresi, 2015]. However, annual-layer dating of the ice core

150    using electrical conductivity (ECM, which is primarily controlled by ice chemistry) and soluble-

151   ion chemistry proved more accurate than dating with visible strata [Buizert et al., 2015; Sigl et al.,

152   2016; WAIS Divide Project Members, 2013]. Here, we estimate the season in which each crust

153   occurs by assigning each summertime peak in the WD2014 time scale to January 1of its year, and

154   then linearly interpolating; accumulation at the site is relatively evenly distributed through the

155   year, justifying this approximation [Banta et al., 2008; Fegyveresi, 2015, Fegyveresi et al., 2016].

156

157   **3: Observations**

158   **3.1: Near-surface observations**

159          We summarize key observations on crust formation here. Additional information, and

160   complete narrative descriptions of particular crust-forming episodes, are provided in Fegyveresi

161   [2015].

162          Glazed crusts were repeatedly observed to form on the snow surface (Figs. 3 and 4),

163   primarily during late-December and January, with an interval between formation events of

164   roughly one and two weeks (see Figs. 5-8). Crust formation often followed a storm or wind event,

165   and occurred during a time of higher atmospheric pressure, light winds, clear sky, strong

166   insolation, large diurnal temperature cycling, and low relative humidity.

167          As shown in Figure 9, the crusts were often internally complex. The upper few

168   millimeters of the surface snow were anomalously high-density (> 400 kg m$^{-3}$) and fine-grained,

169   and might be termed a multi-grain crust. Within this, and especially at the top, were one or more

170   lower-porosity single-grain crusts. To an observer, light reflected off these crusts gave the

171   appearance of a glaze on the snow surface. (e.g. Fig. 4), [see also Orsi et al., 2015, their Fig. 5].

172          Typically, a glazed crust started as isolated sub-meter to few-meter patches on unshaded

173   regions of the snow surface or sastrugi, which were most consistanly exposed to sunlight, and

174   spaced tens of meters to more than 100 m apart. The spatial size and extent of glazed crust

175   patches varied considerably and were not measured directly; however, no single observed crust

176    patch was greater than 100 m in length in any dimension. Over the first days of formation, glazed

177    crusts expanded to form a laterally extensive interconnected surface broken by isolated sub-meter

178    to few-meter unglazed patches on shaded faces of sastrugi. Glazed crusts were most continuous

179    where the surface was smoothest. Reconnaissance surveys extending a few kilometers from camp

180    showed that glazed-crust formation was consistent at least that far.

181         Within 2-3 days of formation, glazed features developed prominent polygonal cracks

182    with few-meter spacing (e.g. Fig. 4). It is likely that these cracks formed by thermal contraction

183    during nighttime cooling, which was driven by the large diurnal temperature swings observed at

184    the time (see below). We excavated some cracks, which could be traced downward from the

185    surface typically ~20-30 cm.

186         A pronounced hoar began forming within 24 hours of the onset of cracking of the glazed

187    crust in each case observed (e.g. Fig. 3). Measured relative humidity was notably higher during

188    hoar formation (see Figs. 5-8) than before, and sometimes (e.g., January 7th, 2010) a fog

189    developed early in the time of hoar formation, providing a source of vapor to the surface hoar

190    from above. Surface glazing was not required for formation of such hoar layers, as one formed

191    quickly on December 30th, 2009 during a very warm (> -10°) fog episode with elevated measured

192    relative humidity, but without prior formation of surface glaze.

193         Hoar layers that we observed during the field seasons were subsequently either buried,

194    destroyed by wind, or gradually sublimated away over 2-3 additional days. We observed strong

195    winds remove hoar layers, with a threshold of ~7 m s$^{-1}$ (~13 knots). In one case, hoar removal

196    required somewhat lower speed when wind was directed orthogonal to the prevailing direction

197    and thus sastrugi orientation, similar to observations by Champollion et al. [2013] at Dome C,

198    East Antarctica.

199         No above-freezing temperatures were observed by the AWS, but on January 2, 2011, the

200    temperature reached a high of -2.8ºC (see Fig. 6; Supplemental Fig. S1). While no direct surface

201 melt was observed, some melt was noted along exposed, vertically cut wall faces near the ice-

202 core drilling facility (Supplemental Fig. S2). A prominent multi-grain crust was observed the next

203 year in snow pits, likely dates from that time, and shows features that are consistent with some

204 melting-refreezing having occurred (Supplemental Fig. S3).

205      The PRD strings document strong variations in subsurface temperature, following the air

206 temperatures as expected. During the cooling phases of diurnal cycles, air temperatures (AWS)

207 and near-surface snow temperatures (S0) dropped well below temperatures deeper in the snow

208 including the shallowest in-snow sensor (S1) at ~20 cm (Figs. 10 and 11), with the surface as

209 much as 3ºC colder than snow at 40 cm (S2) depth (e.g. Supplemental Fig. S4). This would have

210 driven upward mass flux from the deeper snow towards the surface. Such conditions often

211 developed when surface hoar was forming from fog, and thus likely with a downward as well as

212 an upward vapor source to the near-surface layer.

213

214 **3.2: Snow-pit observations**

215      Each of the five snow pits showed a clear annual cycle in the visual stratigraphy, but with

216 notable "noise". Depth hoars occurred primarily in summertime layers and into autumn, but with

217 occasional hoar layers in winter and spring layers. Crusts were also most common in summertime

218 and into autumn, but not restricted to those times. Similar to the observations made by Alley

219 [1988] at other sites in Antarctica, sequences of strata at WAIS Divide typically showed lateral

220 continuity over 2 m scales, although with some variation. Many graded beds were also present,

221 likely indicative of changes during a specific storm event or primarily before the next storm. This

222 was later confirmed on-site with accumulation stakes and measurements following specific large

223 storm events [see also Koffman et al., 2014; Criscitiello et al., 2014].

224      The snow pits from the 2008-09, 2009-10, and 2010-11 seasons at WAIS Divide were

225 mapped here in greatest detail, and meter-wide sub-swaths of their complete pit-wall maps are

226   shown in Figure 12. Complex stratigraphy and variations are clearly discernable, and illustrate the

227   variability within 1 km of each other at WAIS Divide in contiguous years. This is likely

228   indicative of the influence of complex processes of deposition and metamorphism, with frequent

229   occurrences of depositional and erosional features (sastrugi, whalebacks, wind scoops, hollows,

230   etc.). We chose annual layers in the pit maps based upon visual inspection in the field, subsequent

231   examination of photographs of the pits, and overall trends in measured densities (see e.g. Fig. 13).

232       We measured pit bulk densities using 100 $cm^3$ stainless-steel, box-type cutters [e.g.,

233   Conger and McClung, 2009] and a digital scale accurate to 1 gram. Density samples were taken

234   in all five concurrent seasons' pits in duplicate, at ~5 cm intervals, from the pit side-wall (so as

235   not to disturb the back-lit wall). These duplicates were then averaged together for final values.

236   Samples measured in the 2008-09 pit were taken with regards to marked strata, and therefore at a

237   slightly higher frequency. Density measurements from pits of all five seasons yielded an average

238   density of $386.6 \pm 3.2$ kg $m^{-3}$ for the upper 2 meters of snow (Fig. 14), all with a nearly identical

239   linear trend-line slope of ~0.4 kg $m^{-3}$ $cm^{-1}$ with depth.

240       Seasonal interpretations of all five pits indicated an average of ~3.75 years of

241   accumulation recorded over the 2 meter depths, which yields an average of ~0.53 m $a^{-1}$ of

242   accumulation at the average pit snow-density. Converted to water-equivalent, this becomes ~0.20

243   m $a^{-1}_{w.e.}$ (or ~0.22 m $a^{-1}_{ice}$). These values agree closely with recently published values [WAIS

244   Divide Project Members, 2013; Banta et al., 2008; Burgener et al., 2013].

245       We documented obvious crusts and hoar layers for each snow pit. Most commonly, crusts

246   occurred just above depth hoars, but crusts were observed without hoar, and hoar without crust.

247   Both single-grain-thick (~1 mm) and multi-grain ($\geq$4 mm) crusts were observed, with the

248   common association of single-grain crusts in and usually at the top of multi-grain crusts as noted

249   above. All crusts had densities estimated over 400 kg $m^{-3}$. Counting a multi-grain crust containing

250    a single-grain crust as one feature, the five 2-meter snow pits revealed an average of ~18.8 ± 2.5

251    (±1σ) total crusts, or approximately 5 crusts per year.

252    **3.3: Ice-core data**

253    In the bubbly ice included in our crust logging (120-577 m depth) in the WAIS Divide

254    core, 10,268 crusts were identified (Fig. 15). A few were discontinuous across the core, or

255    displayed at least a few pores extending through; others appeared largely or completely

256    continuous and impermeable at the scale of the core. Experience with independent observers

257    showed little or no error in crust identification. We cannot rule out the possibility that bubble

258    migration contributed to loss of some crusts in the deepest bubbly ice considered, but the crusts

259    continued to be clear and readily identifiable, so we do not believe that the trend to fewer crusts

260    in the deepest ice is an artifact. We cannot fully exclude the possibility that there is an

261    observational bias related to the drop in crust prevalence over the most recent ~250 years, as the

262    crusts are more difficult to discern in the shallow firn and snow.

263    The seasonal distribution of the crusts is shown in Figure 16. Crusts occur year-round,

264    but are ~45% more frequent in summertime accumulation than in wintertime. Certainly, the

265    natural variability in seasonal distribution of snow accumulation and in the timing of peak

266    impurity input mean that details of the shape of the seasonal distribution of crust occurrence are

267    notably uncertain. However, given the high reliability of the annual-layer dating, and the multiple

268    indicators that agree well [Buizert et al., 2015; Sigl et al., 2016; WAIS Divide Project Members,

269    2013], "summer" versus "winter" or "nonsummer" is well-constrained.

270    Time-trends of seasonal crust occurrence are also shown in Supplemental Figure S5,

271    separating the largely sunless winter (May-August) from the sunny spring-summer-fall

272     (September-April, with at least 8 hours of sunlight per day). Both first increase and then decrease

273     slightly over the 2400-year record, but with a larger relative change in the sunlight season.

274

275

276     **4: Synopsis and Discussion**

277     Our observations confirm and extend prior work on this topic [see e.g. Anderson and

278     Benson, 1963]. Depositional processes and metamorphism primarily in the upper few centimeters

279     of near-surface snow, produce prominent layering. Wintertime accumulation, while notably

280     variable, is more homogeneous than summertime deposits, with wind-packed layers prominent in

281     winter, and more-variable layers including crusts and hoar more common in summer [e.g., Sorge,

282     1935; Benson, 1962, Gow, 1965; 1969; Weller, 1969; Colbeck, 1982; Colbeck, 1983; Alley,

283     1988; Alley et al., 1997]. These features are altered during subsequent burial and conversion to

284     bubbly ice, but still produce recognizable features in the ice core that allow identification of

285     annual layers and crusts [e.g., Alley et al., 1997; Fitzpatrick et al., 2014].

286     Our observations at WAIS Divide show repeating events that generate the main features

287     of the summertime accumulation. In a typical event, a storm with strong winds brings snow

288     accumulation, followed by a high-pressure system bringing clear skies, greatly reduced winds,

289     initially low humidity, and strong diurnal variations in sunshine, air temperature, and net surface

290     energy-balance.

291     Early in this clear-sky interval, the wind-packed upper surface develops a millimeter-

292     thick glazed crust or possibly crusts in a few-millimeters-thick multi-grain crust. Strengthening of

293     crusts over one to a few days is followed by polygonal cracking from contraction caused by

294     nighttime cooling. Vapor released through the cracks contributes to rising relative humidity, and

295     surface-hoar deposition in subsequent nights. At WAIS Divide, evolution of the crust-hoar

296     complex typically is truncated by arrival of another storm, which may remove or bury the hoar,

297    and typically buries the crusts below the level of fastest metamorphism, allowing them to be

298    preserved.

299         Not every aspect of a typical event is observed in each case. Crusts form and can be

300    buried by additional snowfall without growth of a surface hoar on top of them. Crusts are

301    somewhat discontinuous, and surface hoar can grow where a crust is absent. And, perhaps most

302    importantly here, a crust that remains near the surface (in the upper few centimeters) for too long

303    may slowly lose mass and cease to be a crust.

304         Our data provide strong constraints on models of many of the observed processes.

305    Surface hoar grew especially at night when relative humidity was high, sometimes with fog, and

306    with deposition occurring on tent ropes or other surfaces as well as on the snow surface (e.g.

307    Supplemental Fig. S6), clearly demonstrating a source of vapor from above. Surface hoar

308    typically formed however, when the upper snow surface was colder than layers beneath,

309    indicating a vapor source from below. Hence, our surface hoars included elements of both

310    depositional and sublimation hoar crystals as defined by Gallet et al. [2014] based on

311    observations at Dome C, East Antarctica (with sublimation growth being the dominant process).

312         The high density of both single-grain and multi-grain crusts, approaching the density of

313    ice for the glassy single-grained crusts, requires that the density of the crusts was increased over

314    time, as wind packing has not been observed to approach these high densities. Crusts form during

315    days when atmospheric humidity is low, however, and thus when mass is not being added from

316    above. We have not observed bulk melting at the site (with the one possible exception noted

317    above), nor do the gas measurements of Orsi et al. [2015] indicate bulk melting, so the density

318    increase must arise from some combination of vapor diffusion from below and surface or volume

319    mass transfer likely involving pseudo-liquid layers [Dash et al., 2006], as discussed next.

320         The data here show that frequently the upper surface is colder than snow beneath, which

321    will lead to upward mass flux. We lack subcentimetric resolution in thermometry, but physical

322    understanding indicates that very strong gradients likely develop on the centimeter scale just

323    below the upper surface during rapid nighttime cooling. Physical understanding, the data here,

324    and data from previously published studies indicate that intense sunshine generates a temperature

325    maximum in the snow just below the surface (order of 1 cm) especially in low-density, low-

326    thermal-conductivity depth hoar [e.g., Alley et al., 1990; Brandt and Warren, 1993], also

327    contributing to upward vapor transport. Hence, the upper surface is expected to gain mass from

328    below during the crust- and hoar-forming events [Alley et al., 1990]. Windy conditions would

329    drive undersaturated air into and out of pore spaces, removing mass, but crusts form during

330    relatively still times. The temperature gradients (and noted inversions) measured here at WAIS

331    Divide (see also Figs. 10 and 11, and Supplemental Fig. S4) are similar to those observed at

332    GISP2 by Alley et al. [1990] and more than sufficient to move the necessary vapor for crust

333    development.

334          We hypothesize here that these surface conditions cause mass fluxes that fill in open

335    pores in wind-packed layers at the surface to form glazed crusts. A physical model might be

336    based on the following considerations. The thermal conductivity of ice greatly exceeds that of air,

337    so heat transport in near-surface snow is primarily conductive. Ordinarily, the grain curvature

338    adjacent to pores tends to cause diffusive mass loss, enlarging pores by filling necks between

339    grains or other regions of lower vapor pressure. However, because heat flow is primarily through

340    the grain structure, pores in a surface crust will tend to be colder than interconnected grains when

341    the upper surface is colder than the snow beneath, favoring mass transport to the pore surfaces, as

342    shown in Figure 17 [e.g., Sommerfeld, 1983; Fukuzawa and Akitaya, 1993]. Transport may occur

343    by vapor, surface, or volume diffusion; following Alley and Fitzpatrick [1999], vapor diffusion

344    and surface transport in premelted films are likely to dominate. Also, mass loss from relatively

345    warm grain bonds just beneath a growing surface crust by diffusion to the colder crust will tend to

346   lower the crust, increasing the likelihood that a pore in the crust will move downward to intersect

347   a pre-existing grain beneath, increasing the crust density.

348       Due to the inherent limitations with the available sensor equipment, and with the sparsity

349   of usable data for our specific periods of interest, a complete and detailed analysis of radiative

350   forcings was not completed here. However, to further test our hypothesis and to assess the

351   accuracy of our measurements, we did execute a simple surface energy budget (SEB) calculation

352   in order to solve for the ground heat flux term $Q_G$, and ultimately determine if the AWS sensor

353   data yield flux rates capable of the hypothesized vertical vapor transport in the near-surface snow.

354   Because data from the AWS-mounted net radiometer and thermistor strings were only available

355   for the 2012-13 field season, only that specific time window was used for this simple SEB

356   calculation (see also Figs. 8 and 10).

357       The surface energy budget represents a balance of turbulent, radiative, and ground heat

358   fluxes, which are all coupled through various processes [see e.g. Hulth et al, 2010; Miller et al.,

359   2017]. Because there is no known or observed melting at the WAIS Divide site, and therefore no

360   phase changes in the near-surface snow, a change in any of the SEB terms is thus balanced by

361   changes in other terms. For simplicity, we represent this relationship here as:

362   $$Q_N + Q_S + Q_L + Q_G = 0 \tag{1}$$

363   $$Q_N = S_{NET} + L_{NET} = S\downarrow + S\uparrow + L\downarrow + L\uparrow \tag{2}$$

364   where $Q_N$ is the total net radiation ($S_{NET}$ and $L_{NET}$ are the net short and longwave radiation terms),

365   $Q_S$ and $Q_L$ are the sensible and latent turbulent heat fluxes respectively, and $Q_G$ is the ground heat

366   flux. The net radiation term $Q_N$ was determined by combining the short and longwave radiation

367   data obtained directly from the radiometer (see Fig. 8). Due to limitiations with the Kipp-Zonen

368   CNR2 sensor, only the radiative *NET* terms were available, and not the individual incoming ($\downarrow$)

369   and outgoing ($\uparrow$) terms.

370     Based upon the Monin-Obukhov similarity theory, the sensible and latent heat flux terms

371     can be expressed as:

372     $$Q_S = \rho c_p u_* T_* \ \ and \ \ Q_L = \rho L_S u_* q_*$$     (3)

373     where $\rho$ denotes air density, $c_p$ is the specific heat of dry air at constant pressure (1005 J K$^{-1}$ kg$^{-1}$),

374     and $L_S = 2.83 \cdot 10^6$ J kg$^{-1}$ is the latent heat of sublimation. We use bulk method approximations for

375     the turbulent scales of wind speed ($u_*$), temperature ($T_*$), and humidity ($q_*$), and their related

376     stability correction functions [Van As et al., 2005; Andreas, 2002; Fairall et al., 1996; Holtslag

377     and DeBruin,1988]. We also employed an optimal velocity roughness length (~0.03 mm) and

378     calculated the related roughness terms using published equations [Miller et al., 2017; Van As et

379     al., 2005; Andreas, 1987]. As previously noted, relative humidity values reported here are

380     expressed in terms of saturation vapor pressure over ice and corrected for low-temperature offsets

381     [see Anderson, 1994]. Specific humidity is calculated from relative humidity using published

382     equations [Van As et al., 2005].

383     Results of this SEB calculation are shown in Supplemental Fig. 7, and values for ground

384     heat flux were determined by solving equation (1) for $Q_G$. Over the ~24 hr, low-wind period

385     shown highlighted in Figure 8 that features a surface glaze (labeled 'b'), the net ground heat flux

386     $Q_G$ does corroborate a condition favorable for upward (negative) energy flux, particularly during

387     the morning hours of the 24-DEC-2012.

388     We calculated thermal conductivity of the uppermost snow layers as $K = 0.35 \pm 0.05$

389     Wm$^{-1}$ K$^{-1}$, from our measured snow pit density data (see Fig. 14), combined with published

390     relations between density and $K$ [Miller et al., 2017; Jordan, 1991]. Then, we used $K$, $Q_G$, and the

391     equation for conductive heat flux,

392     $$Q_G = -K\frac{\Delta T}{\Delta z}$$     (4)

393     to calculate vertical temperature difference ($\Delta$T), over the top 20 cm ($\Delta$Z) [Van As et al., 2005].

394    Our results yield an average vertical temperature difference of ~3.6 ± 0.7 ºC over the ~24

395    hr, low-wind, glaze period highlighted in Figure 8, or a gradient of ~18 ºC m$^{-1}$. This result is

396    consistent with the thermistor string data (see Figs. 10 and 11), which indicate a temperature

397    difference between the near-surface air sensor (AWS), and the shallowest in-snow sensor (S1, 20

398    cm depth) of ~3.0ºC during the peak of the inversion and glazing episode on 24-DEC-2012; the

399    near-surface air sensor was ~1 m above the surface, and we infer that, as a result, it somewhat

400    underestimated peak ΔT.

401    Our energy-balance calculation, although simple, retains the key physics and follows

402    earlier work. We thus trust the basic result, with agreement between model and measured

403    temperatures, that the energy balance generates sufficient heat fluxes to drive the vapor mass

404    transport needed for glazed-crust development [Pinzer et al., 2012]. We are confident that a more-

405    comprehensive study extending this work would be instructive, with additional sampling and

406    modeling addressing the overall radiative and SEB responses, boundary-layer stability responses,

407    cloud forcings, and vapor mass flux rates.

408    Although summertime crusts dominate in the ice core, many wintertime crusts were

409    identified, raising additional questions. We lack direct observations in winter, and so can only

410    speculate on mechanisms active then. However, the basic picture drawn above for summertime

411    crusts may also apply in winter. The lower temperatures, and lack of intense solar heating, make

412    crust formation less likely. However, stronger wintertime winds would allow greater wind-

413    packing of the upper surface, producing fewer and smaller pores to be filled to make a thin crust,

414    and thus making crust formation easier. Although accumulation is more-or-less evenly distributed

415    through the year, long periods of limited variability observed in AWS data suggest that there may

416    be extended intervals up to weeks in length during the winter when the surface is relatively stable,

417    partially or completely offsetting the slower mass transport from colder temperatures.

418    Furthermore, the AWS data show that mid-winter temperatures have risen as high as -15°C

419  during strong warming events accompanied by high winds ($> 10$ m s$^{-1}$), and likely linked to

420  transport of air masses from the coast. Such warm air masses paired with these high winds would

421  produce relatively high vapor pressures, contribute to greater surface packing, and promote

422  temperature inversions and upward near-surface vapor flux during the subsequent cooling.

423      The great abundance of crusts at WAIS Divide compared to other ice cores we have

424  studied may be because conditions are "just right" at WAIS Divide. We have observed loss of a

425  wind-packed crust at WAIS Divide, and also at GISP2 in central Greenland; the strong mass loss

426  from the upper ~1 cm of the snowpack is not conducive to long-term survival of any crust there

427  [e.g., Alley et al., 1990]. Low but nonzero summertime accumulation thus may lead to loss of

428  crusts, whereas higher accumulation after formation buries them below that zone of mass loss and

429  so allows their preservation. The large wintertime variability and high wintertime temperatures at

430  WAIS Divide may be important in generating sufficiently high mass fluxes to produce wintertime

431  crusts.

432      At least in summertime, crusts do seem to record a particular meteorological pattern of

433  storms alternating with still conditions. The time-series of frequency of occurrence of crusts thus

434  would be affected by a change in the frequency of occurrence of these conditions. Turning this

435  into a paleoclimatic indicator would require additional steps, however, as the frequency of

436  preserved crusts could decrease because fewer were formed or because more were destroyed,

437  with different causes. Information on changing frequency of meteorological events might be

438  useful [e.g., Hammer, 1985; Alley, 1988]. We believe that the clear association of crust formation

439  with particular events, and the clear trends in crust occurrence in the core, motivate additional

440  research on topics including crust formation in non-summer seasons, but we do not know whether

441  this ultimately could yield a valuable paleoclimatic indicator.

442     **5: Conclusions**

443             Summertime observations at the WAIS Divide site show that prominent visible strata

444     form at or very near the surface during summer, by processes that typically are repeated a few

445     times during each summer. A storm produces a wind-packed layer. The following high-pressure

446     system brings light winds, warm days and cool nights, strong sunshine, and low relative

447     humidity. High-density, single-grain-thick glazed crusts preferentially form at the surface during

448     these high-pressure intervals, in as little as a single day, and then strengthen and evolve. Crusts

449     are extensive, although typically broken by sub-meter or few-meter uncrusted regions spaced tens

450     of meters to more than 100 m apart. Daytime solar heating drives upward mass transport to crusts

451     from developing depth hoar beneath, strengthening the crusts. A simple surface energy budget

452     (SEB) calculation shows that sufficient vertical heat fluxes exist to explain both the observed

453     near-surface temperature inversions, and the vapor mass-flux necessary for the associated glazed-

454     crust formation. After formation, crusts are broken by polygonal cracks extending typically 20-30

455     cm deep, likely from contraction during nighttime cooling. Relative humidity then rises in the air

456     above, contributing to growth of surface hoar during nighttime cooling. Subsequent storms

457     typically bury the crust-hoar complexes, although crusts can be lost during evolving surface

458     conditions if not buried below the top one to a few centimeters.

459             Study of the WAIS Divide deep core shows that crusts are preserved through the bubbly

460     ice. Crusts are most common in layers deposited during summertime, but also occur in winter

461     accumulation. Study of AWS data suggests that the intrusion of warm coastal air during winter

462     may generate strong temperature gradients, which may contribute to wintertime crust formation

463     in wind-packed layers.

464             The frequency of occurrence of crusts in the core varies with time, suggesting the

465     possibility that crusts could be used as a paleoclimatic indicator. However, additional work would

466    be required, including addressing whether crust frequency varies because of changes in formation

467    or changes in destruction of crusts previously formed. The crusts do not produce significant

468    anomalies in other ice-core paleoclimatic records, likely at least in part because they are

469    discontinuous and broken by contraction cracks.

470    **6: Data Availability:**

471        Data policy: All data presented here are available via download from NSIDC

472    (http://nsidc.org) or from the WAIS Divide data portal (http://waisdivide.unh.edu).

473

474    **7: Author Contribution:**

475        A.J. Orsi assisted with field observations and experiments. A. Muto designed the near-

476    surface PRD sensor strings and developed the associated logging code. M. Spencer documented

477    all ice-core crust observations during the WAIS Divide core processing at the National Ice Core

478    Laboratory. J.M. Fegyveresi and R.B. Alley prepared the manuscript with contributions from all

479    co-authors.

480

481   **8: Acknowledgements:**

482        We acknowledge the following funding sources for support of this work: U.S. National

483   Science Foundation Division of Polar Programs grants 0539578, 1043528, 1142085, 1619793.

484   We also acknowledge Donald E. Voigt, Joan J. Fitzpatrick, Eric D. Cravens, and the staff of the

485   U.S. National Ice Core Laboratory in Denver, Colorado, as well as the WAIS Divide Science

486   Coordination Office at the University of New Hampshire, and the Ice Drilling Design and

487   Operations group at the University of Wisconsin. We thank numerous colleagues involved with

488   the WAIS Divide project, especially Kendrick Taylor, Mark Twickler, and Joseph Souney. We

489   thank Bess Koffman, Gifford Wong, Dominic Winski, Aron Buffen, and Logan Mitchell for

490   assistance with snow pit preparation. We thank Jonathan Thom and the University of Wisconsin-

491   Madison Automatic Weather Station Program for assistance with weather station sensor

492   installation. Lastly, we thank our reviewers, whose thoughtful suggestions and questions served

493   to clarify and improve this manuscript. Any use of trade, firm, or product names is for descriptive

494   purposes only and does not imply endorsement.

495

496

**9: References**

Alley, R.B., 1988. Concerning the deposition and diagenesis of strata in polar firn. *J. of Glaciology*, 34: 283-290, doi:10.3189/S0022143000007024.

Alley, R.B., Saltzman, E.S., Cuffey, K.M. and Fitzpatrick, J.J., 1990. Summertime formation of depth hoar in central Greenland. *Geophysical Research Letters*, *17*(13): 2393-2396, doi:10.1029/GL017i013p02393.

Alley, R.B. and Fitzpatrick, J.J., 1999. Conditions for bubble elongation in cold ice-sheet ice. *J. of Glaciology*, *45*(149): 147-153, doi:10.3189/S0022143000003129.

Alley, R.B., Shuman, C.A., Meese, D.A., Gow, A.J., Taylor, K.C., Cuffey, K.M., Fitzpatrick, J.J., Grootes, P.M., Zielinski, G.A., Ram, M. and Spinelli, G., 1997. Visual–stratigraphic dating of the GISP2 ice core: Basis, reproducibility, and application. *J. of Geophysical Research: Oceans*, *102*(C12): 26367-26381, doi:10.1029/96JC03837.

Anderson, P.S., 1994. A method for rescaling humidity sensors at temperatures well below freezing. *J. of Atmospheric and Oceanic Technology*, *11*(5): 1388-1391, doi:10.1175/1520-0426.

Anderson, D. L., and Benson C.S., 1963, The densification and diagenesis of snow, in Ice and Snow: Properties, Processes and Applications, edited by W. D. Kingery, pp. 391–411, MIT Press.

Andreas, E.L., 1987. A theory for the scalar roughness and the scalar transfer coefficients over snow and sea ice. *Boundary-Layer Meteorology*, 38(1):159-184, doi:10.1007/BF00121562.

Andreas, E.L., 2002. Parameterizing scalar transfer over snow and ice: a review. *J. of Hydrometeorology*, 3(4): 417-432, doi:10.1175/1525-7541.

Banta, J.R., McConnell, J.R., Frey, M.M., Bales, R.C. and Taylor, K., 2008. Spatial and temporal variability in snow accumulation at the West Antarctic Ice Sheet Divide over recent centuries. *J. of Geophysical Research: Atmospheres*, *113*(D23), doi:10.1029/2008JD010235.

Battle, M.O., Severinghaus, J.P., Sofen, E.D., Plotkin, D., Orsi, A.J., Aydin, M., Montzka, S.A., Sowers, T. and Tans, P.P., 2011. Controls on the movement and composition of firn air at the West Antarctic Ice Sheet Divide. *Atmospheric Chemistry and Physics*, *11*(21): 11007-11021, doi:10.5194/acp-11-11007-2011.

Benson, C.S., 1962. Stratigraphic Studies on Greenland Ice Sheet and a Quantitative Classification of Glaciers. *Bulletin of the American Meteorological Society*, *43*(4): 141.

Brandt, R.E. and Warren, S.G., 1993. Solar-heating rates and temperature profiles in Antarctic snow and ice. *J. of Glaciology*, *39*(131): 99-110, doi:10.3189/S0022143000015756.

Buizert, C. et al., 2015. The WAIS Divide deep ice core WD2014 chronology–Part 1: Methane synchronization (68–31 ka BP) and the gas age–ice age difference. *Climate of the Past*, *11*(2): 153-173, doi:10.5194/cp-11-153-2015.

Burgener, L., Rupper, S., Koenig, L., Forster, R., Christensen, W.F., Williams, J., Koutnik, M., Miege, C., Steig, E.J., Tingey, D., Keeler, D., and Riley, L., 2013. An observed negative trend in Antarctic accumulation rates from 1975 to 2010: Evidence from new observed and simulated records. *J. of Geophysical Research-Atmospheres*, 118(10): 4205-4216, doi:10.1002/jgrd.50362.

Champollion, N., Picard, G., Arnaud, L., Lefebvre, E. and Fily, M., 2013. Hoar crystal development and disappearance at Dome C, Antarctica: observation by near-infrared photography and passive microwave satellite. *The Cryosphere*, *7*(4): 1247-1262, doi:10.5194/tc-7-1247-2013.

544    Colbeck, S.C., 1982. An overview of seasonal snow metamorphism. *Reviews of Geophysics*,
545          *20*(1): 45-61, doi:10.1029/RG020i001p00045.
546    Colbeck, S.C., 1983. Theory of metamorphism of dry snow. *J. of Geophysical Research: Oceans*,
547          *88*(C9): 5475-5482, doi:10.1029/JC088iC09p05475.
548    Conger, S.M., McClung, D.M., 2009. Comparison of density cutters for snow profile
549          observations. *J. of Glaciology*, 55(189): 163-169, doi:10.3189/002214309788609038.
550    Criscitiello, A.S., Das, S.B., Karnauskas, K.B., Evans, M.J., Frey, K.E., Joughin, I., Steig, E.J.,
551          McConnell, J.R., and Medley, B., 2014. Tropical Pacific Influence on the Source and
552          Transport of Marine Aerosols to West Antarctica. *J. of Climate*, 27(3): 1343-1363,
553          doi:10.1175/JCLI-D-13-00148.1.
554    Das, S.B. and Alley, R.B., 2005. Characterization and formation of melt layers in polar snow:
555          observations and experiments from West Antarctica. *J. of Glaciology*, *51*(173): 307-312,
556          doi:10.3189/172756505781829395.
557    Dash, J.G., Rempel A.W., and Wettlaufer J.S., 2006. The physics of premelted ice and its
558          geophysical consequences, *Rev. Mod. Phys*. 78, 695-741,
559          doi:10.1103/RevModPhys.78.695.
560    Fairall, C.W., Bradley, E.F., Rogers, D.P., Edson, J.B. and Young, G.S., 1996. Bulk
561          parameterization of air-sea fluxes for tropical ocean-global atmosphere coupled-ocean
562          atmosphere response experiment. *J. of Geophysical Research: Oceans*, 101(C2): 3747-
563          3764, doi:10.1029/95JC03205.
564    Fegyveresi, J.M., 2015, Physical properties of theWest Antarctic Ice Sheet (WAIS) Divide deep
565          core: Development, evolution, and interpretation, PhD thesis, The Pennsylvania State
566          Univ., State College, Pa.
567    Fegyveresi, J.M., Alley, R.B., Fitzpatrick, J.J., Cuffey, K.M., McConnell, J.R., Voigt, D.E.,
568          Spencer, M.K. and Stevens, N.T., 2016. Five millennia of surface temperatures and ice
569          core bubble characteristics from the WAIS Divide deep core, West Antarctica.
570          *Paleoceanography*, *31*: 416–433, doi:10.1002/2015PA002851.
571    Fitzpatrick, J.J., Voigt, D.E., Fegyveresi, J.M., Stevens, N.T., Spencer, M.K., Cole-Dai, J., Alley,
572          R.B., Jardine, G.E., Cravens, E.D., Wilen, L.A. and Fudge, T.J., 2014. Physical
573          properties of the WAIS Divide ice core. *J. of Glaciology*, *60*(224): 1181-1198,
574          doi:10.3189/2014JoG14J100.
575    Fukuzawa, T. and Akitaya E., 1993. Depth-hoar crystal-growth in the surface-layer under high-
576          temperature gradient. *Ann. of Glaciology*, *18*: 39-45, doi:10.1017/S026030550001123X.
577    Gallet, J.C., Domine, F., Savarino, J., Dumont, M. and Brun, E., 2014. The growth of sublimation
578          crystals and surface hoar on the Antarctic plateau. *The Cryosphere*, *8*(4): 1205-1215,
579          doi:10.5194/tc-8-1205-2014.
580    Gow, A. 1965. On the accumulation and seasonal stratification of snow at the South Pole. *J. of*
581          *Glaciology*, *5*(40): 467-477, doi:10.3189/S002214300001844X.
582    Gow, A. 1969. On the rates of growth of grains and crystals in south polar firn. *J. of Glaciology*,
583          *8*(53): 241-252, doi:10.3189/S0022143000031233.
584    Hammer, C.U., 1985. The influence on atmospheric composition of volcanic eruptions as derived
585          from ice-core analysis. *Ann. of Glaciology*, *7*: 125-129,
586          doi:10.1017/S0260305500006029.
587    Holtslag, A.A.M. and De Bruin, H.A.R., 1988. Applied modeling of the nighttime surface energy
588          balance over land. *J. of Applied Meteorology*, 27(6): 689-704, doi:10.1175/1520-0450.
589    Hulth, J., Rolstad, C., Trondsen, K. and Rødby, R.W., 2010. Surface mass and energy balance of
590          Sørbreen, Jan Mayen, 2008. *Ann. of Glaciology*, 51(55): 110-119,
591          doi:10.3189/172756410791392754.

Jordan, R.: A one-dimensional temperature model for a snow cover: Technical documentation for SNTHERM.89, Special Report 91-16, Cold Regions Research and Engineering Laboratory (U.S.) and Engineer Research and Development Center (U.S.), 1991.

Koerner, R.M. 1971. A stratigraphic method of determining the snow accumulation at Plateau Station, Antarctica, and application to South Pole-Queen Maud Land traverse 2, 1965-1966. In Crary, A.P. *Antarctic snow and ice studies II*, (Washington, DC, American Geophysical Union): 225-238.

Koffman, B.G., Kreutz, K.J., Breton, D.J., Kane, E.J., Winski, D.A., Birkel, S.D., and Kurbatov, A.V., 2014. Centennial-scale variability of the Southern Hemisphere westerly wind belt in the eastern Pacific over the past two millennia. *Climate of the Past*, 10(3): 1125-1144, doi:10.5194/cp-10-1125-2014.

Lazzara, M.A., Weidner, G.A., Keller, L.M., Thom J.E., and Cassano, J.J., 2012. Antarctic Automatic Weather Station Program 30 Years of Polar Observations. *Bulletin of the American Meteorological Society*, *93*(10): 1519-1537, doi:10.1175/BAMS-D-11-00015.1.

Miller, N.B., Shupe, M.D., Cox, C.J., Noone, D., Persson, P.O.G. and Konrad, S., 2017. Surface energy budget responses to radiative forcing at Summit, Greenland. The Cryosphere, 11(1): 497-516, doi:10.5194/tc-11-497-2017.

Mitchell, L.E., Buizert, C., Brook, E.J., Breton, D.J., Fegyveresi, J., Baggenstos, D., Orsi, A., Severinghaus, J., Alley, R.B., Albert, M. and Rhodes, R.H., 2015. Observing and modeling the influence of layering on bubble trapping in polar firn. *J. of Geophysical Research: Atmospheres*, *120*(6): 2558-2574, doi:10.1002/2014JD022766.

Muto, A., Scambos, T.A., Steffen, K., Slater, A.G. and Clow, G.D., 2011. Recent surface temperature trends in the interior of East Antarctica from borehole firn temperature measurements and geophysical inverse methods. *Geophysical Research Letters*, *38*(15), doi:10.1029/2011GL048086.

Orsi, A.J., Kawamura, K., Fegyveresi, J.M., Headly, M.A., Alley, R.B. and Severinghaus, J.P., 2015. Differentiating bubble-free layers from melt layers in ice cores using noble gases. *J. of Glaciology*, *61*(227): 585-594, doi:10.3189/2015JoG14J237.

Pinzer, B.R., Schneebeli, M. and Kaempfer, T.U., 2012. Vapor flux and recrystallization during dry snow metamorphism under a steady temperature gradient as observed by time-lapse micro-tomography. *The Cryosphere*, 6(5): 1141-1155, doi:10.5194/tcd-6-1673-2012.

Sigl, M. et al., 2016. The WAIS Divide deep ice core WD2014 chronology–Part 2: Annual-layer counting (0–31 ka BP). *Climate of the Past*, *12*(3):769-786, doi:10.5194/cp-12-769-2016.

Sommerfeld, R.A., 1983. A branch grain theory of temperature gradient metamorphism in snow. *J. of Geophysical Research: Oceans*, *88*(C2):1484-1494, doi:10.1029/JC088iC02p01484.

Sorge, E., 1935. Glaziologische Untersuchungen in Eismitte. *Brockamp, B., and others. Glaziologie. Leipzig, FA Brockhaus*, *935*: 62-270.

Van As, D., Van Den Broeke, M. and Van De Wal, R., 2005. Daily cycle of the surface layer and energy balance on the high Antarctic Plateau. *Antarctic Science*, 17(1): 121-133, doi:10.1017/S095410200500252X.

WAIS Divide Project Members, 2013. Onset of deglacial warming in West Antarctica driven by local orbital forcing. *Nature*, *500*(7463): 440-444, doi:10.1038/nature12376.

Weller, G. 1969. The heat and mass balance of snow dunes on the central Antarctic Plateau. *J. of Glaciology*, *8*: 277-284, doi:10.3189/S0022143000031257.

**Sample ID: WDC05A - 77.260**

10 mm
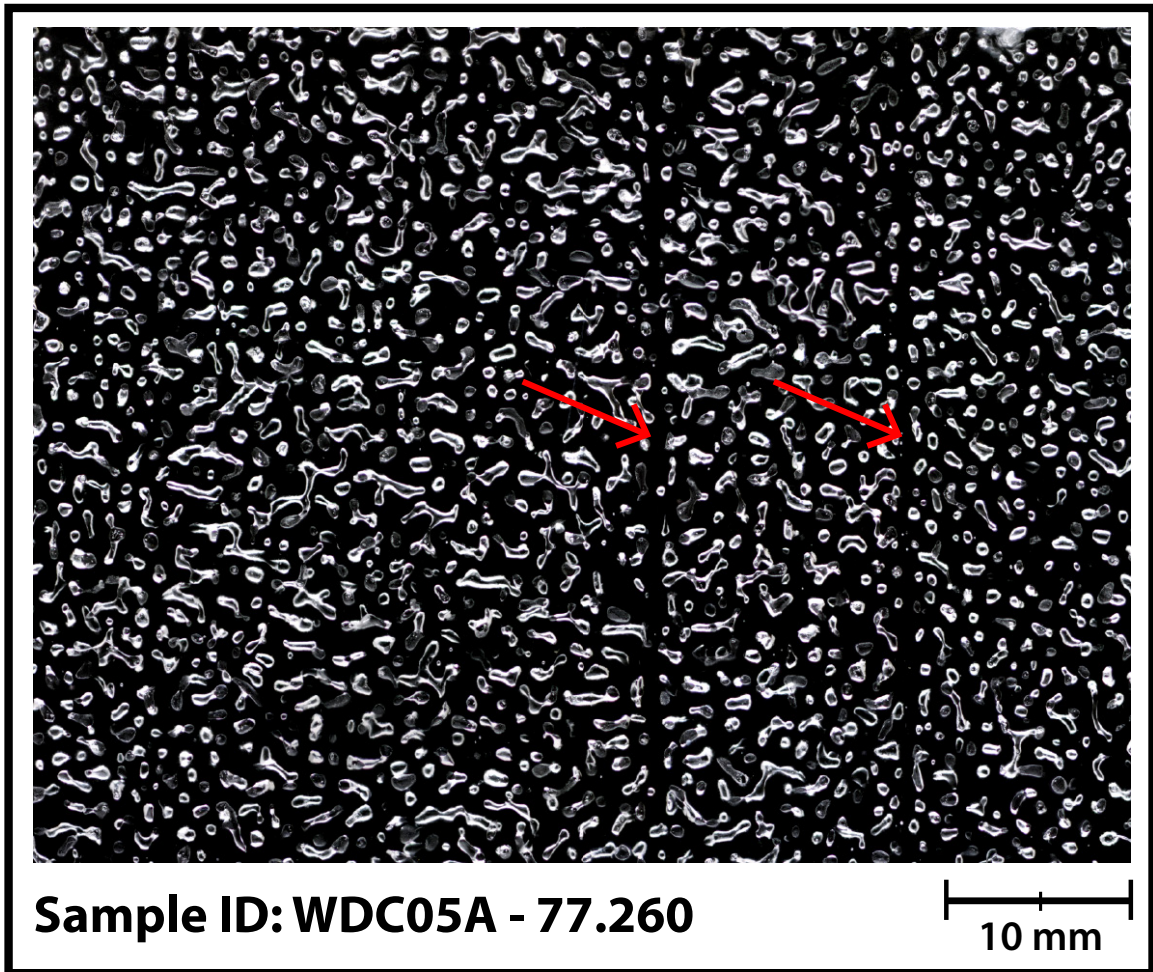
Figure 1: A thick-section image of a sample prepared from a depth of ~77.260 meters showing two preserved crusts. Both layers are ~1 mm thick and appear mostly bubble-free. All bubbles here appear white, with the surrounding ice black. The general elongated shape of the bubbles is due the proximity of this sample to the bubble close-off depth at WAIS Divide of ~75 meters). This sample is from the secondary WDC05A core at the WAIS Divide site. Image modified from Orsi et al. [2015].
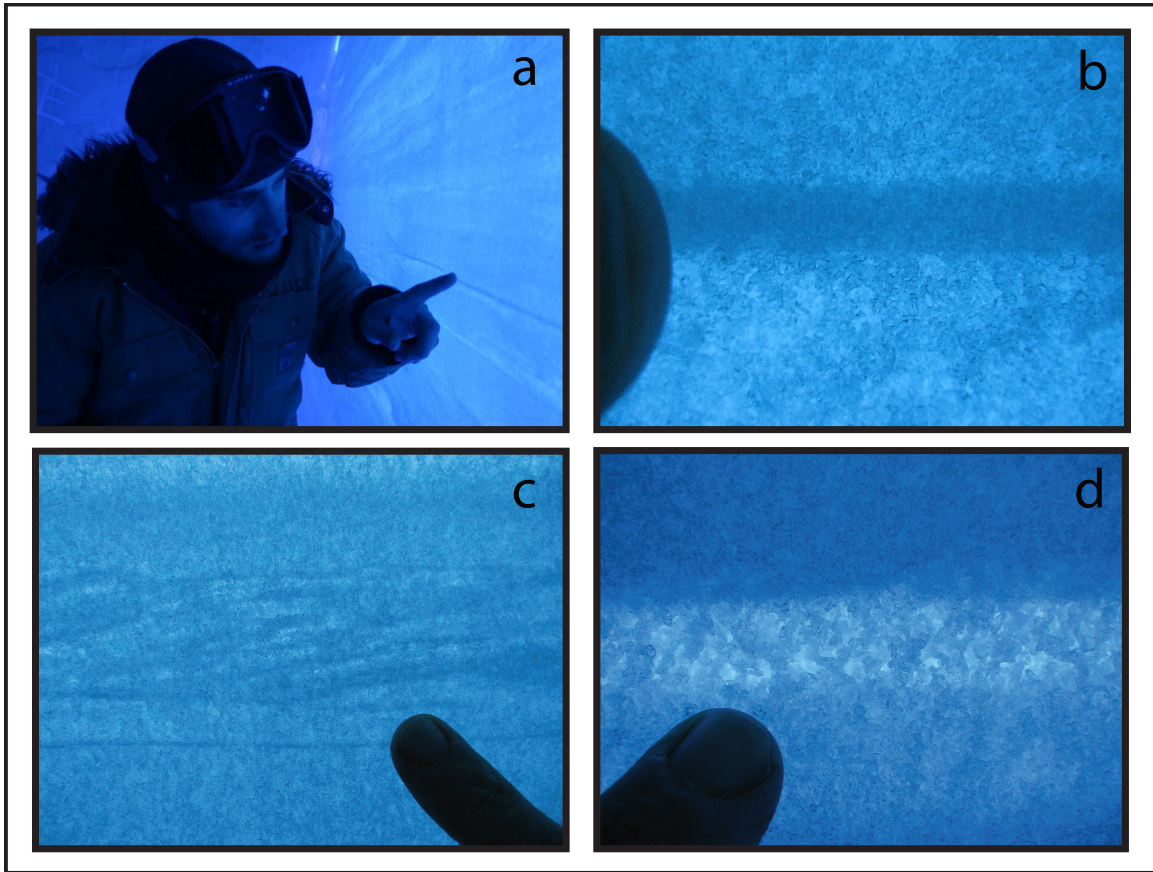
646
647
648 **Figure 2:** The lead author in a 2-meter snow pit prepared at WAIS Divide (pit 2009-10-A).
649 Multi-grain crusts (a, b), preserved sastrugi with cross-bedding (c), and hoar layers (d) are all
650 easily identifiable.
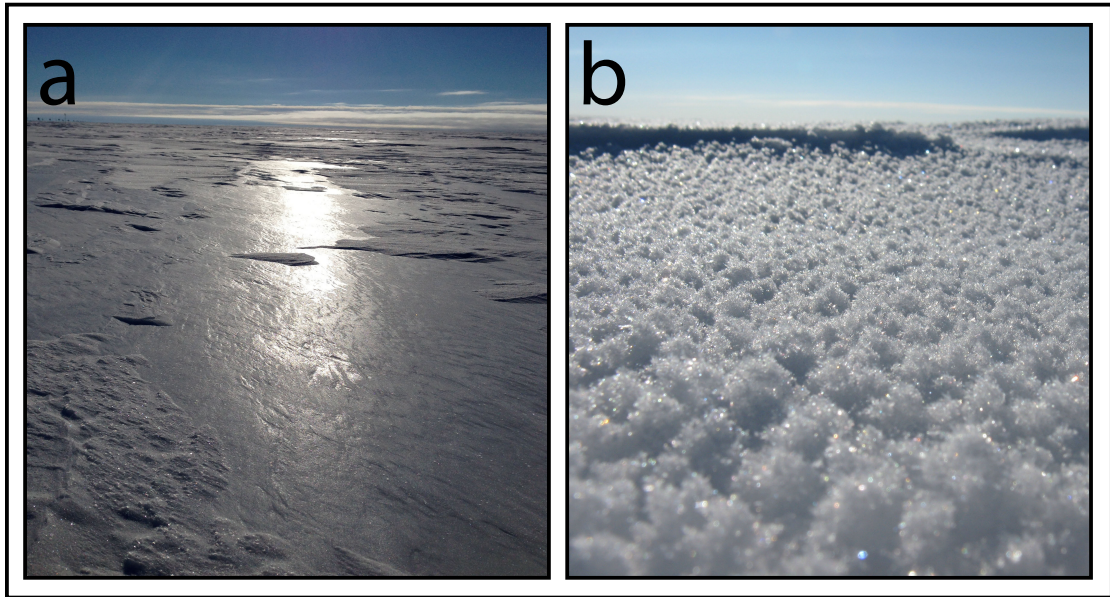
651
652  **Figure 3:** Surface "glaze" (a) that formed on a calm, sunny day (23-Dec-2012) at WAIS Divide,
653  and the subsequent surface hoar layer (b) that formed on its surface after several calm days.
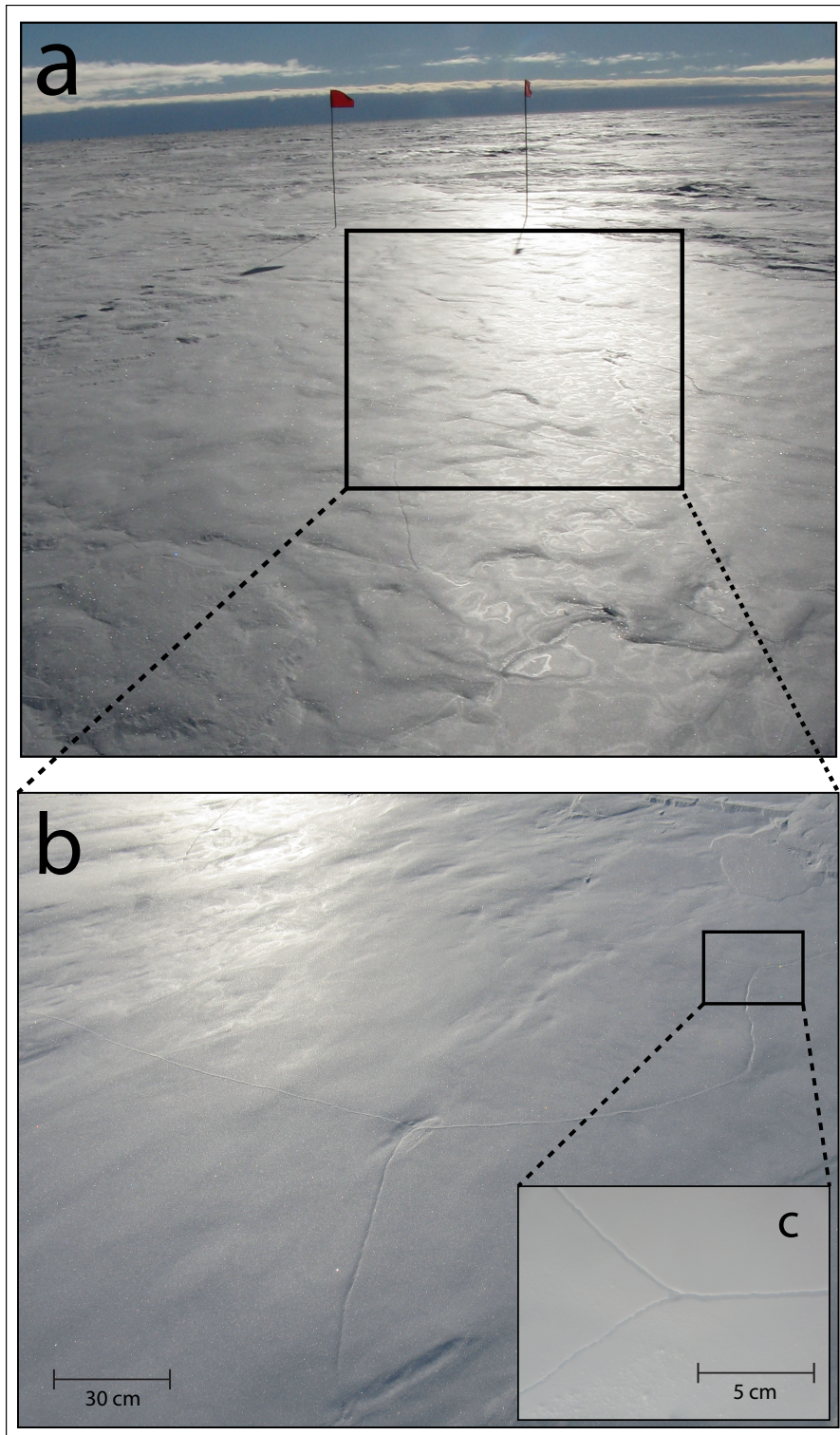
654
655
656    **Figure 4:** Surface "glaze" seen at the WAIS Divide site. (a). A zoomed-in view shows the
657    polygonal cracking that initiates at the surface from thermal contraction, following several sunny,
658    clear-sky days (b). Closer inspection reveals greater detail and scale of a crack triple-junction (c).
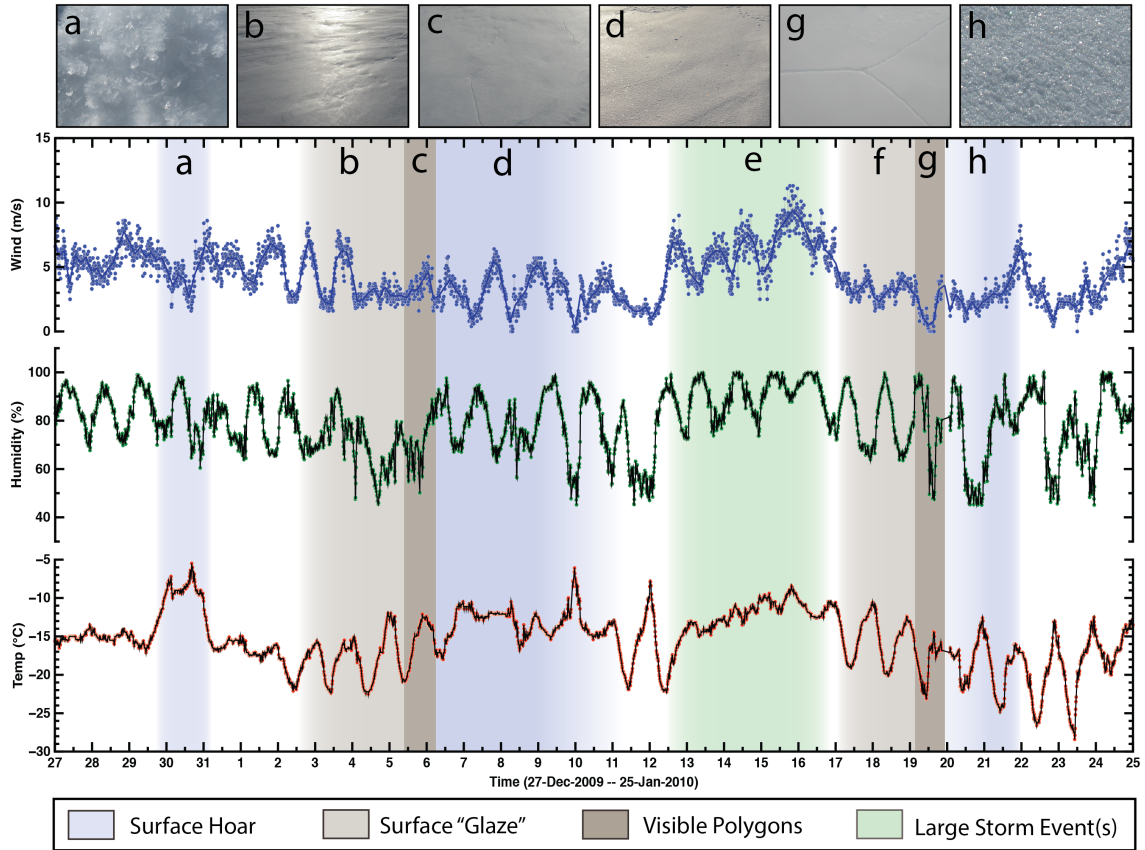
**Figure 5:** Surface evolution over 29 days in 2009-10 season, and AWS data. Shading shows episodes of surface hoar, glazes, and polygonal cracking; storm events are also shown. Letters near the top refer to photographs above of specific features or events. All dates and times are GMT (-12 WAIS local time). The errors for all AWS instruments are listed in Supplemental Table S1.
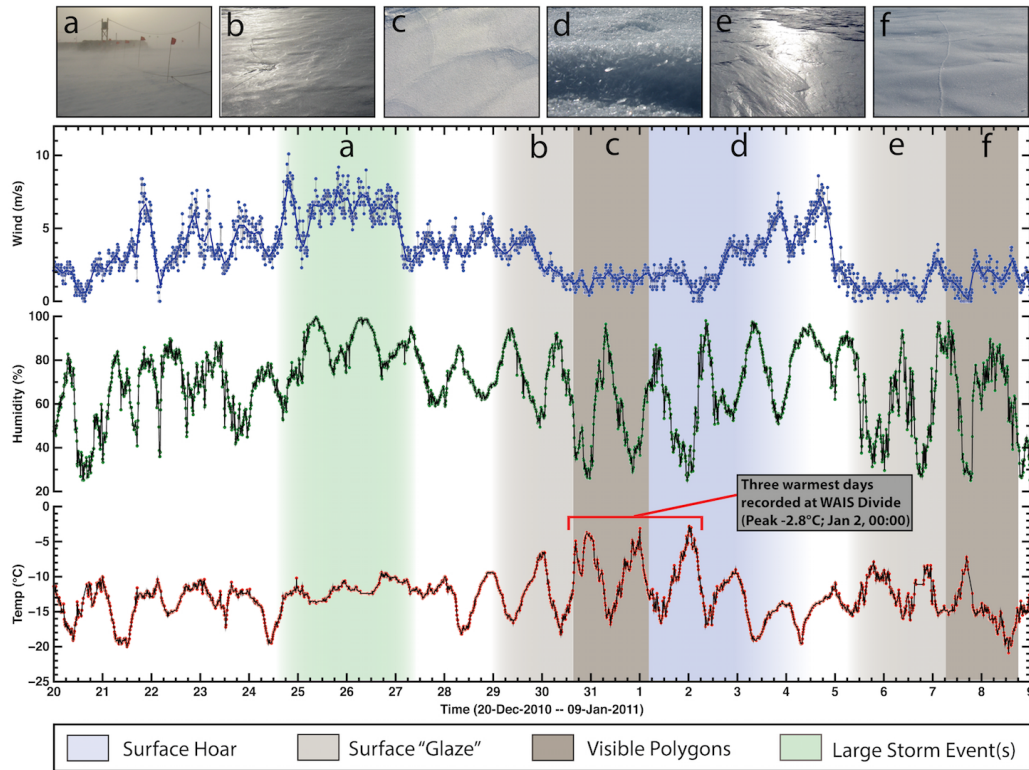
**Figure 6:** Surface evolution over 20 days in 2010-11 season, and AWS data. Shading shows
episodes of surface hoar, glazes, and polygonal cracking; storm events are also shown. Letters
near the top refer to photographs above of specific features or events. All dates and times are
GMT (-12 WAIS local time). The errors for all AWS instruments are listed in Supplemental
Table S1.
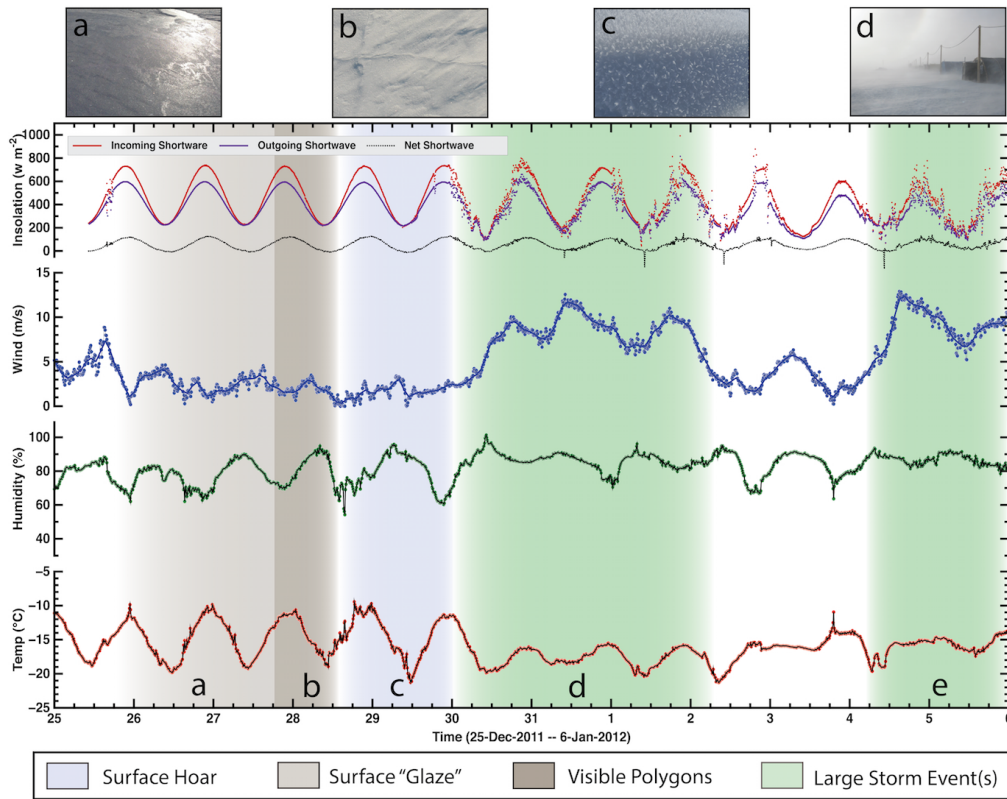
**Figure 7:** Surface evolution over 12 days in 2011-12 season, and AWS data. Shading shows episodes of surface hoar, glazes, and polygonal cracking; storm events are also shown. Letters near the top refer to photographs above of specific features or events. All dates and times are GMT (-12 WAIS local time). The errors for all AWS instruments are listed in Supplemental Table S1.
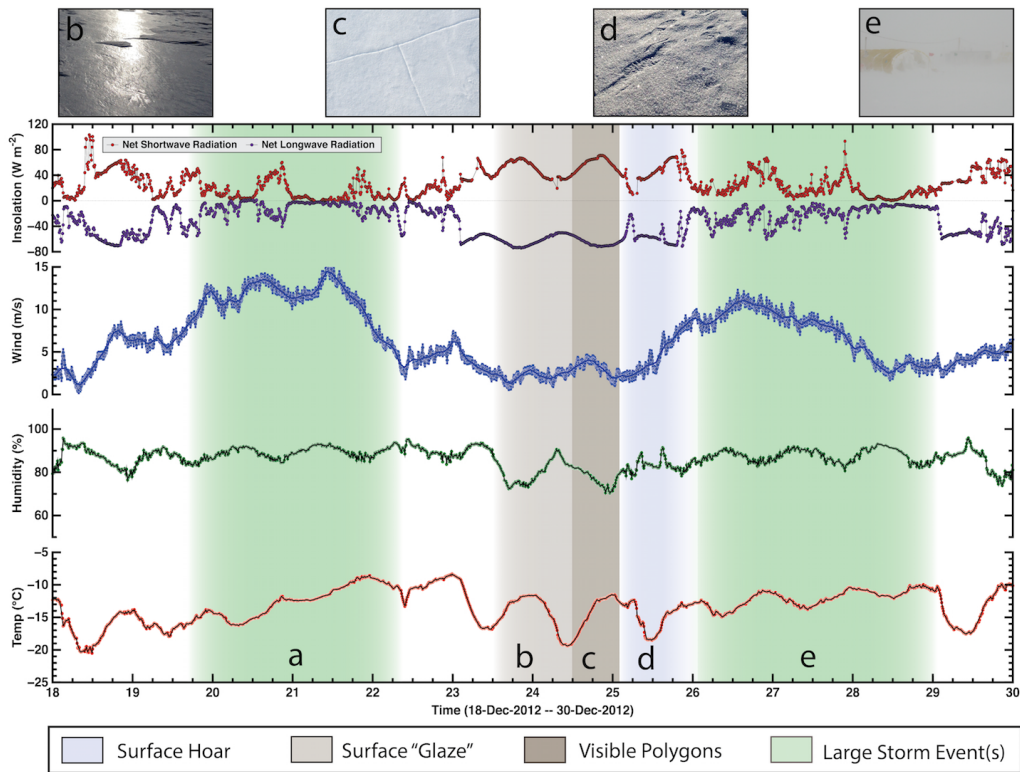
**Figure 8:** Surface evolution over 12 days in 2012-13 season, and AWS data. Shading shows episodes of surface hoar, glazes, and polygonal cracking; storm events are also shown. Letters near the top refer to photographs above of specific features or events. All dates and times are GMT (-12 WAIS local time). The errors for all AWS instruments are listed in Supplemental Table S1.
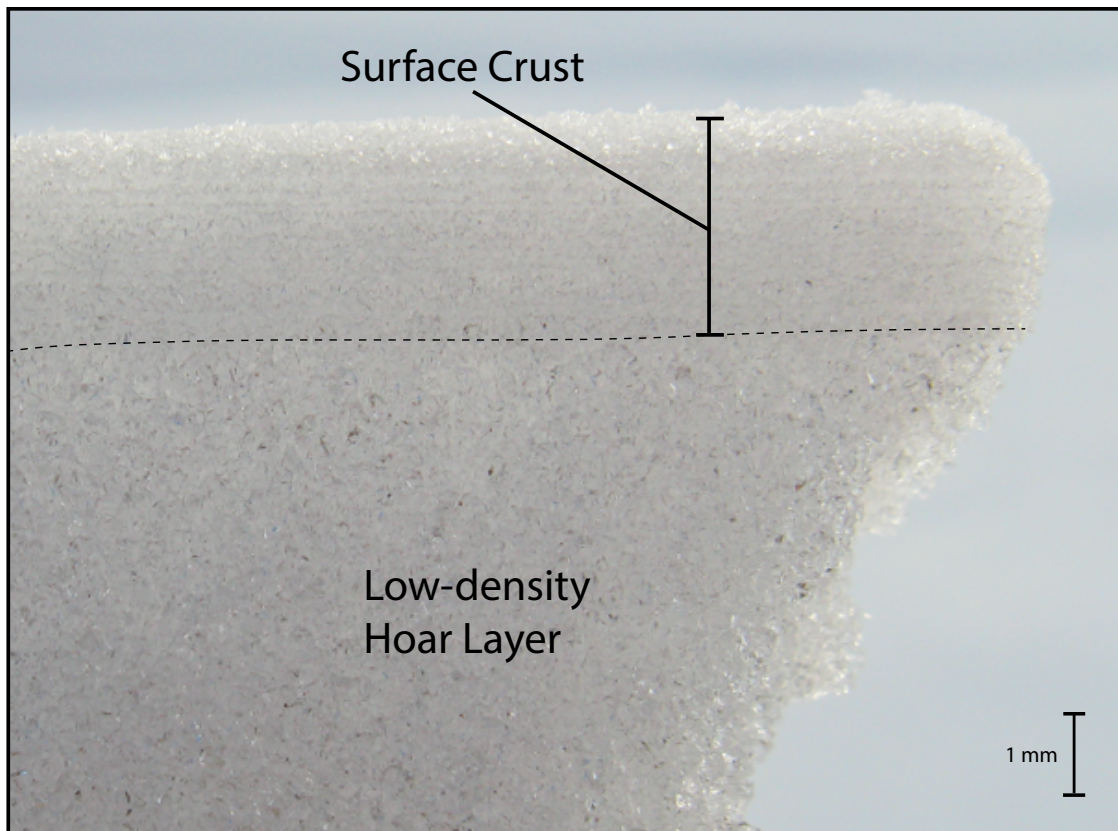
687
688
689 **Figure 9:** A surface snow sample excavated from a glazed area at WAIS Divide before the onset
690 of polygonal cracking, showing a couplet of an evolved high-density (> 400 kg m$^{-3}$), ~3 mm
691 multi-grain surface crust containing single-grain crusts, and overlying a lower-density (< 300 kg
692 m$^{-3}$) hoar layer.
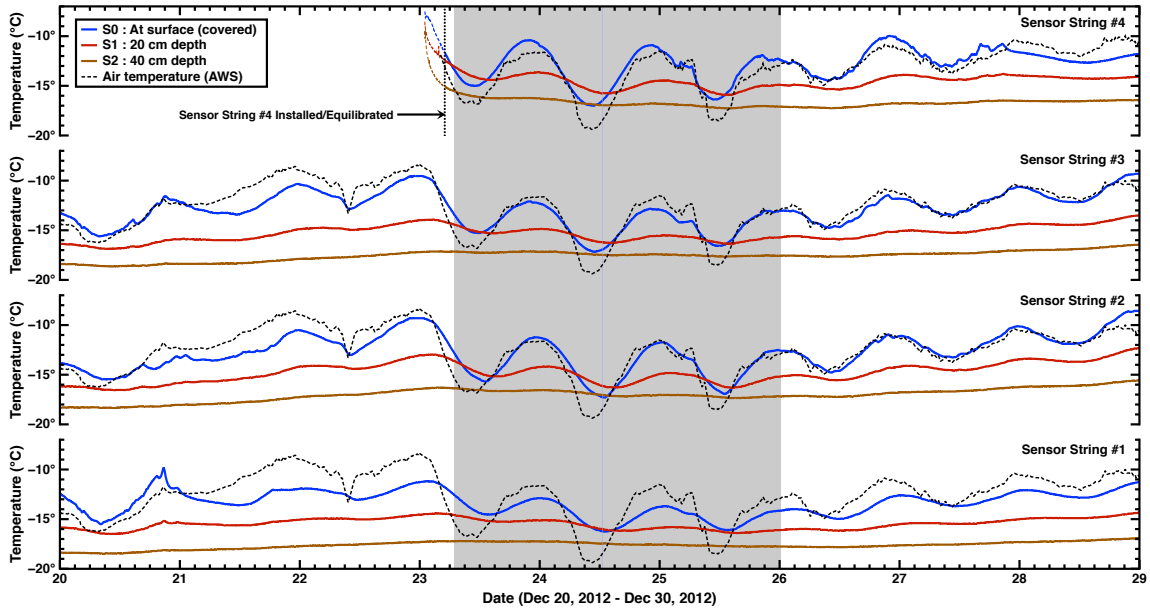
693
694
695 **Figure 10:** Temperature measurements (1 min interval) in snow from the 2012-13 season, from
696 the upper-most three PRDs (surface down to 40 cm). Data are from the four sensor stations
697 closest to the station. The shaded area corresponds to an episode of glaze and hoar growth (see
698 Fig. 8). Distinct near-surface temperature inversions occurred each night during this 3-day period
699 (see Fig. 11). Sensor #4 was not installed until Dec 22nd, and therefore did not equilibrate until
700 early on the 23rd as indicated. Air temperature is also shown as recorded by the AWS (errors
701 listed in Supplemental Table S1). The AWS temperature sensor is located ~1 meter above the
702 snow surface. All dates and times are GMT (-12 WAIS local time).
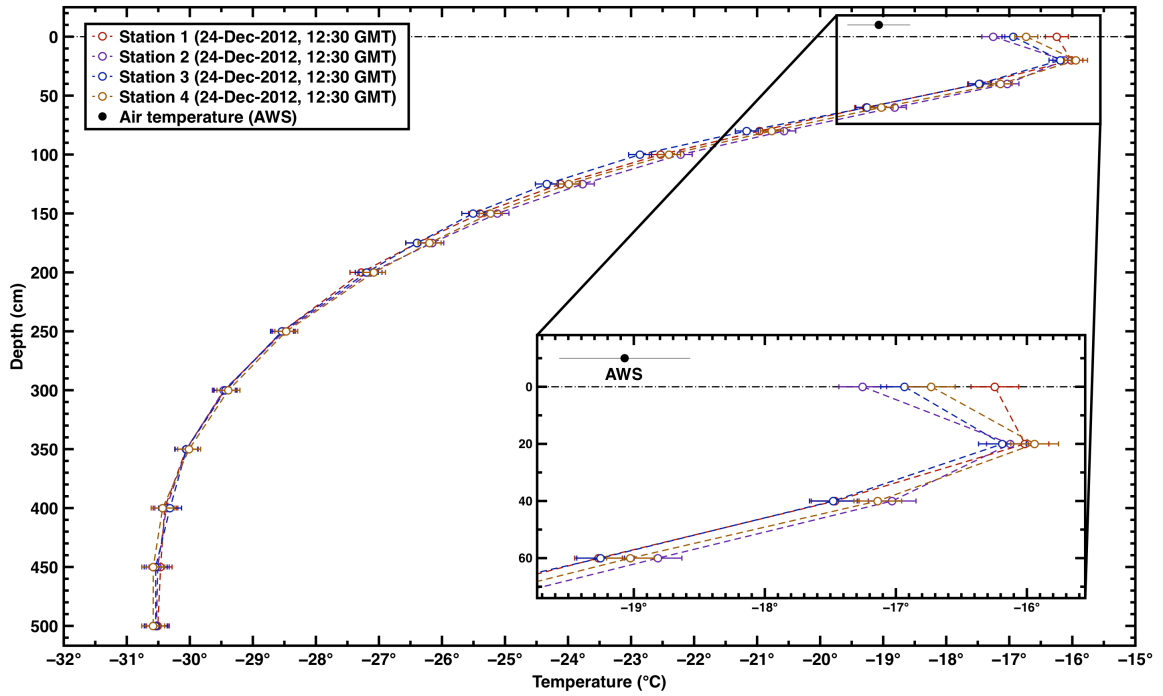
703
704
705 **Figure 11:** Snap-shot temperature readings for PRD-string stations #1-4, taken on 24-Dec-2012
706 at ~12:30 GMT, showing the temperature inversion with colder air (AWS data) and upper surface
707 over warmer near-surface snow.
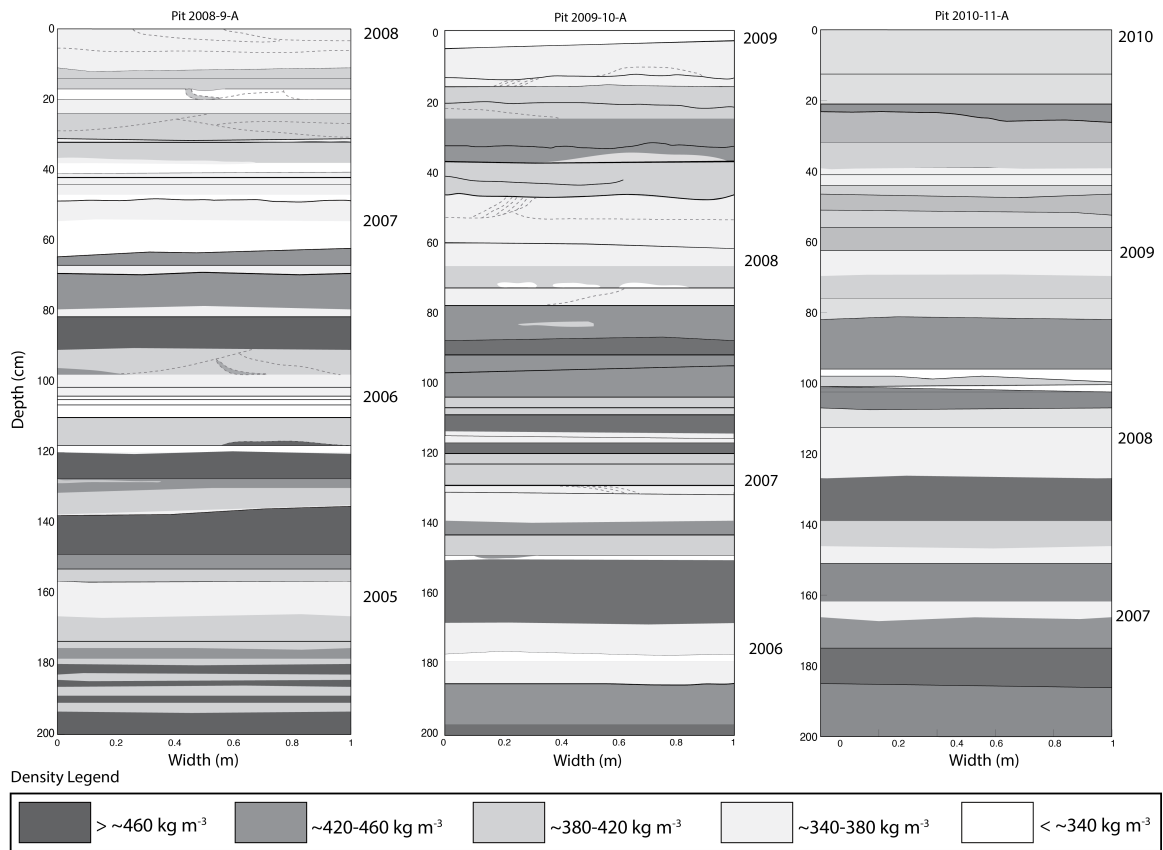
708
709
710 **Figure 12:** Complete wall maps of back-lit snow pits prepared during 2008-09, 2009-10, and
711 2010-11 WAIS Divide field seasons. Layering and density contrast are noted by degree of
712 shading. Fine- to medium- grained, higher-density snow layers are shown with darker grey
713 coloring, whereas coarse-grained and low-density layers (e.g., depth hoar) are shown in white.
714 Crusts are indicated with solid lines, while dotted lines are used to represent cross-bedding at
715 depth. Years were identified based on approximate depths of peak summers and the average
716 measured densities. The pit wall surfaces trend in parallel with the prevailing wind direction at
717 WAIS Divide (approximately north-south, with north to the right).
718
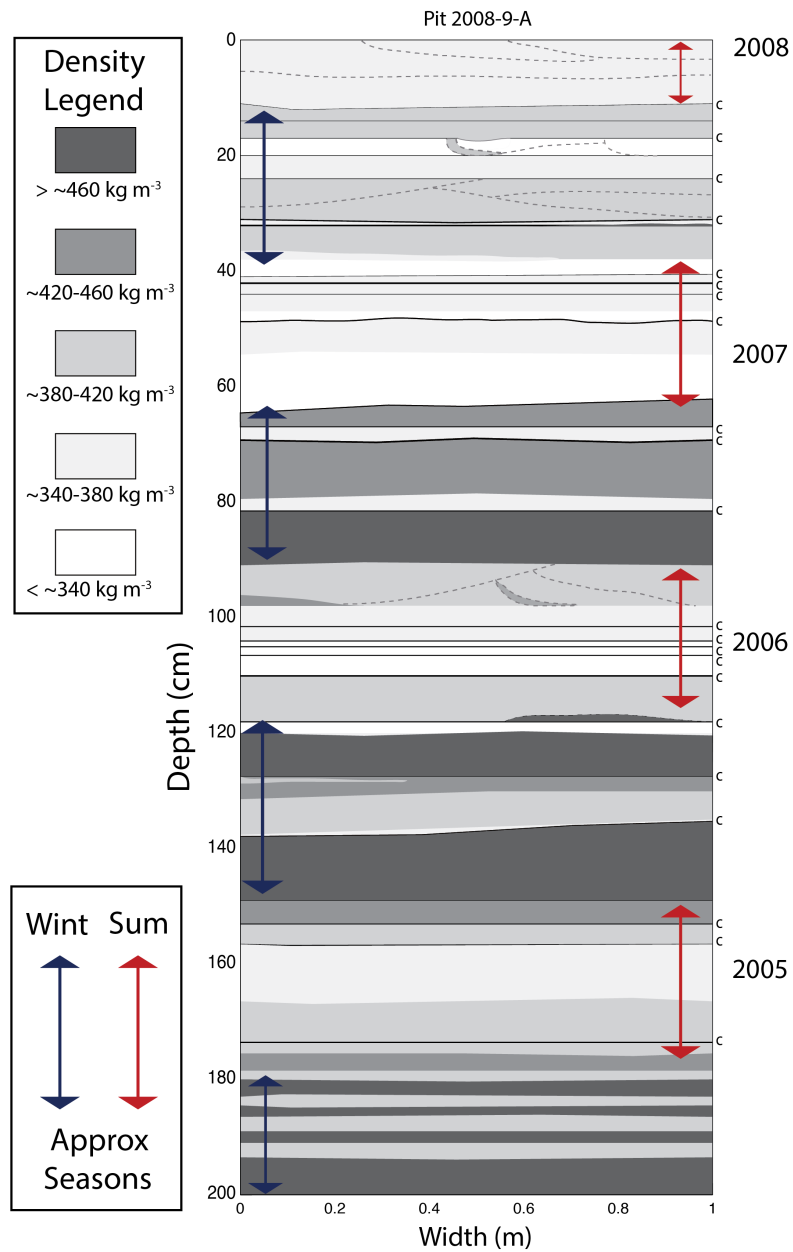
719
720
721 **Figure 13:** A detailed view of data for snow pit 2008-09-A, including wall map, density profile,
722 annual layer picks, and crusts occurrences. Density, layering, and feature preservation are again
723 noted as in Fig. 12. Individual crusts are identified with a labeled "c" along the vertical axis.
724 Seasonal accumulation layers "picked" visually in the pit (shown with red and blue arrows)..
725 These observations indicate a somewhat regular pattern of equally-distributed yearly
726 accumulation at WAIS Divide with clear annual signals.
727
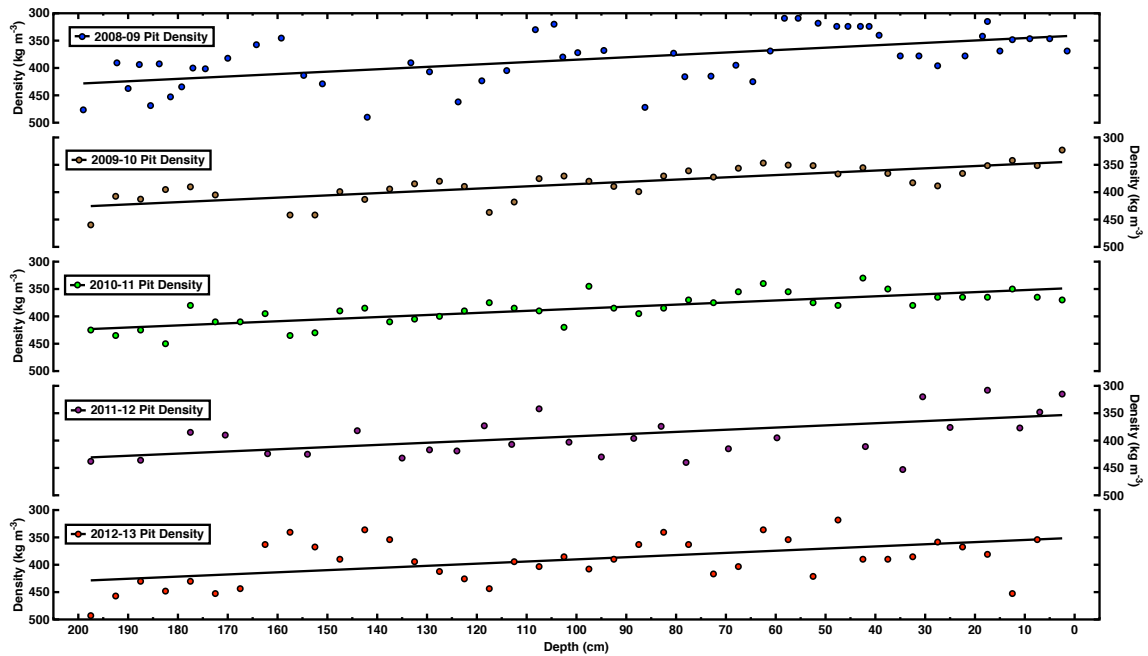
728
729
730 **Figure 14:** Density profiles measured in snow pits from five concurrent seasons at WAIS Divide
731 (2008-2012). Each pit showed a high degree of sample-to-sample variability as measured
732 densities were widely-spaced within the upper 2 meters of snow; estimated annual signals were
733 still identifiable, however. Measurements yielded an overall average density of $386.6 \pm 3.2$ kg m$^{-3}$
734 for the upper 2 meters of snow across all 5 pits, with nearly identical linear trend-line slopes of
735 ~0.4 kg m$^{-3}$cm$^{-1}$ with depth.

736
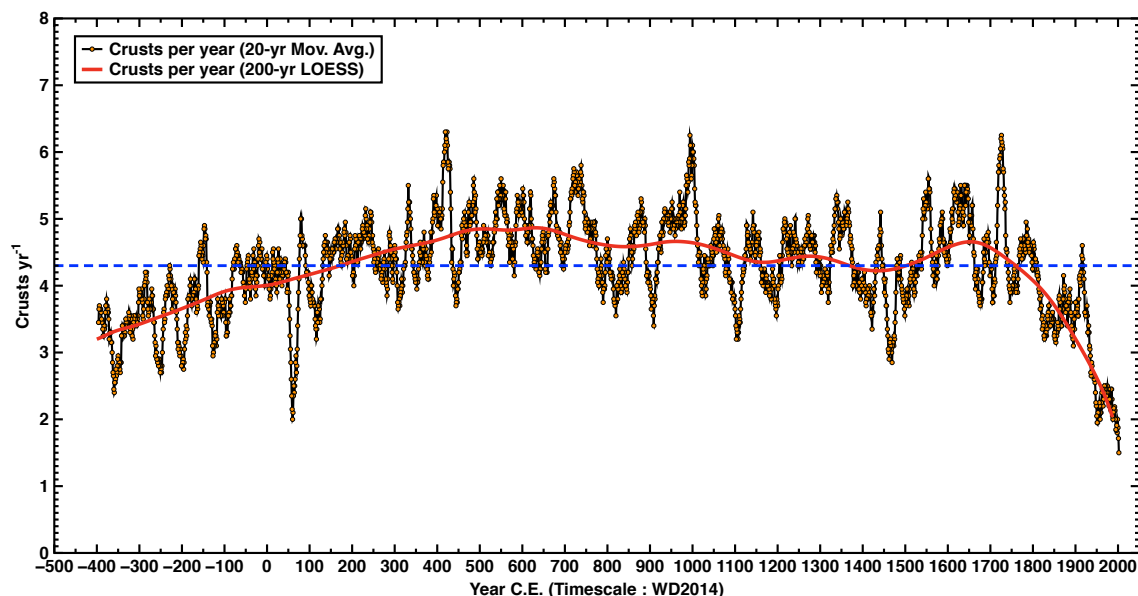
737
738
739 **Figure 15:** History of crust occurrence (crusts year[-1]) in the bubbly-ice zone of the WDC06A
740 core that we studied in detail (~120 – 577 m depth); ages (C.E.) are from the WD2014 depth-age
741 scale). 10,268 unique crusts were documented in the core, for an average rate of 4.3 ± 2 per year
742 (dashed blue line). Data are shown as 20-yr moving averages for ease of view, with an added 1st-
743 order LOESS smoothing trend-curve (200-yr bin-width). The sharp decline in crust prevalence
744 after ~1750 C.E. may be due to observational biasing in the shallow firn and snow.
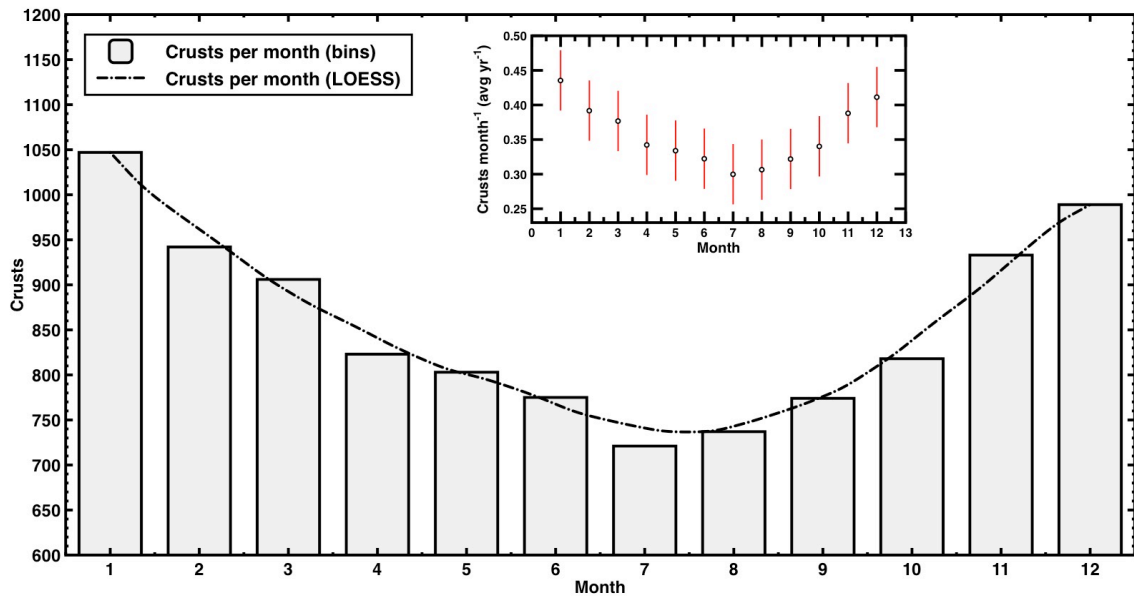
745
746
747 **Figure 16:** Crust distribution by month (1=January, 2=February,…12=December) based on
748 assumption that each summer pick in the WD2014 depth-age scale is January 1, and then
749 interpolating linearly. Crusts occur year-round but more commonly in summer accumulation. The
750 smoothed curve is a 1$^{st}$-order LOESS trend curve (width = 2). Data shown for 2400-yr record.
751 Inset shows average crusts per month (±1σ).
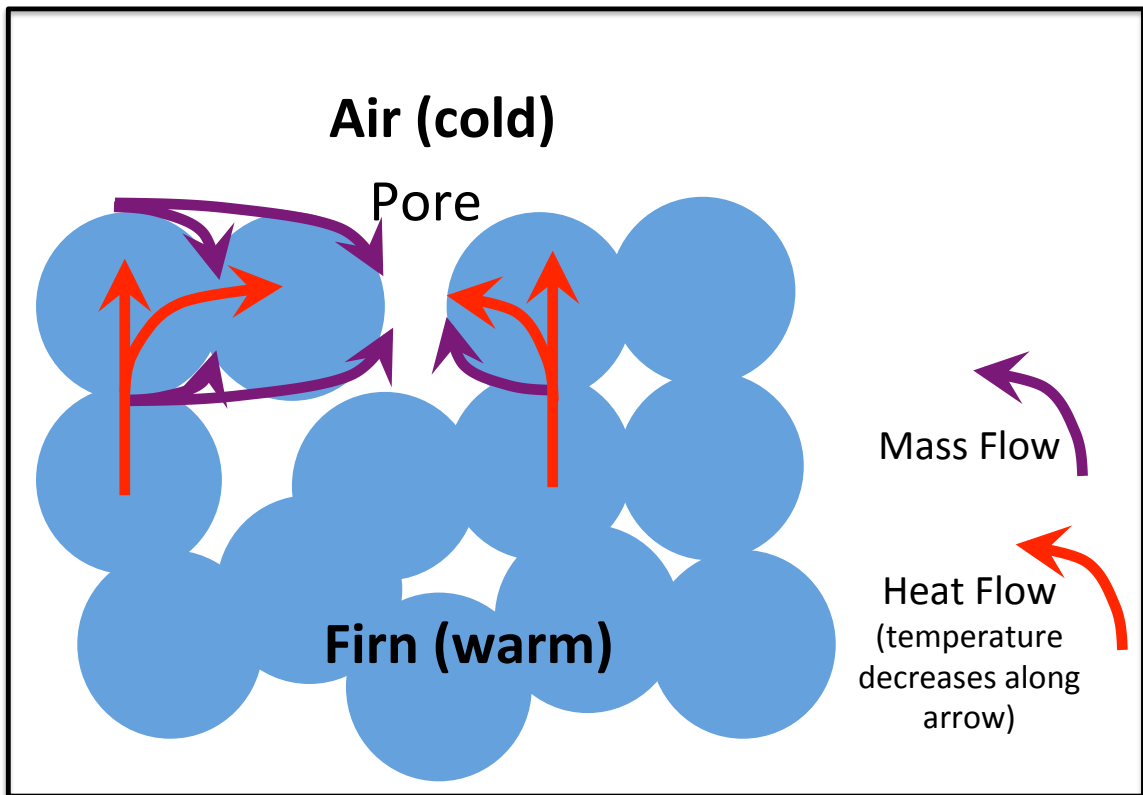
752
753
754 **Figure 17:** Schematic illustrating possible mass and heat transports during during formation of a
755 single-grain glazed crust, when the near-subsurface is warmer than the surface. Heat flow is
756 primarily through the grain structure (blue), so pores (white) in the surface layer will be colder
757 than interconnected grains, favoring mass transport from the grains to those pores, increasing
758 density of the surface layer.
759

760 **Table 1:** Field observation table (see also Figs. 5, 6, 7, 8).

| Field Season | Observation Window | Observation Duration | AWS | Other Instrumentation | Pit |
|---|---|---|---|---|---|
| 2008-2009[1] | 12-Dec-2008 : 10-Jan-2009 | ~29 days | -- | -- | x |
| 2009-2010[1] | 27-Dec-2009 : 25-Jan-2010 | ~29 days | W,H,T | -- | x |
| 2010-2011 | 20-Dec-2010 : 09-Jan-2011 | ~20 days | W,H,T | -- | x |
| 2011-2012[1] | 25-Dec-2011 : 04-Jan-2012 | ~12 days | W,H,T,I | Dual Li-Cor LI200 sensors | x |
| 2012-2013[1] | 18-Dec-2012 : 30-Dec-2012 | ~12 days | W,H,T,I | Kipp-Zonen CNR2 sensor Shallow PRD strings[2] | x |

W,H,T,I - Wind, Humidity, Temperature, Insolation
[1]Fegyveresi, 2015
[2]Muto et al., 2011

761